Article

Remote Inspection of Bridges with the Integration of Scanning Total Station and Unmanned Aerial Vehicle Data

Piotr Olaszek [1,*] , Edgar Maciejewski [2], Anna Rakoczy [2], Rafael Cabral [3], Ricardo Santos [4]
and Diogo Ribeiro [4]

1   Road and Bridge Research Institute, ul. Instytutowa 1, 03-302 Warszaw, Poland
2   Faculty of Civil Engineering, Warsaw University of Technology, al. Armii Ludowej 16, 00-637 Warsaw, Poland;
     edgar.maciejewski.stud@pw.edu.pl (E.M.); anna.rakoczy@pw.edu.pl (A.R.)
3   CONSTRUCT-LESE, Department of Civil Engineering, University of Porto, R. Dr. Roberto Frias s/n,
     4200-465 Porto, Portugal; up201609762@edu.fe.up.pt
4   CONSTRUCT-LESE, Department of Civil Engineering, Polytechnic of Porto, R. Dr. António Bernardino de
     Almeida 431, 4249-015 Porto, Portugal; rps@isep.ipp.pt (R.S.); drr@isep.ipp.pt (D.R.)
*   Correspondence: polaszek@ibdim.edu.pl

Abstract: Remote visual inspections are valuable tools for maintaining bridges in safe operation. In the case of old structures with incomplete documentation, the verification of dimensions is also an essential aspect. This paper presents an attempt to use a Scanning Total Station (STS) and Unmanned Aerial Vehicle (UAV) for the inspection and inventory of bridge dimensions. The STS's measurements are conducted by applying two methods: the direct method using a total station (TS) and advanced geometric analyses of the collected point cloud. The UAV's measurements use a Structure from Motion (SfM) method. Verification tests were conducted on a steel truss railway bridge over the largest river in Poland. The measurements concerned both the basic dimensions of the bridge and the details of a selected truss connection. The STS identified a significant deviation in the actual geometry of the measured connection and the design documentation. The UAV's inspection confirmed these findings. The integration of STS and UAV technologies has demonstrated significant advantages, including STS's high accuracy in direct measurements, with deviations within acceptable engineering tolerances (below a few mm), and the UAV's efficiency in covering large areas, achieving over 90% compliance with reference dimensions. This combined approach not only reduces operating costs and enhances safety by minimizing the need for heavy machinery or scaffolding but also provides a more comprehensive understanding of the structural condition.

Keywords: visual inspections; Scanning Total Station (STS); Unmanned Aerial Vehicle (UAV); Structural Health Monitoring (SHM); damage identification

1. Introduction

The increasing number of old and deteriorated bridge structures around the world has significantly fostered the importance of their inspection and maintenance. Traditional visual inspections supplemented with remote structural health monitoring (SHM) methods are valuable tools to keep bridges safely in service. In the case of old structures with incomplete documentation, the verification of dimensions is also an essential aspect. Traditional on-foot or on-boat visual inspections have many limiting factors. For large or tall structures, there is little to no possibility of visually inspecting the entire structure without using boom lifts or other heavy machinery, which increases the associated operation costs and risks.

Many researchers and industrial centers around the world are working on the use of modern techniques for remote inspection of bridges [1]. Nepomuceno et al. [2] present a possible diagram for remote visual inspections. They emphasize that the risk to inspectors' health and safety would be reduced when they are not required to be on-site. On-site photographers (with the use of a 360° camera) are expected to spend less time on-site than

a traditional inspector. Galdelli et al. [3] and Ribeiro et al. [4] present a remote visual inspection system for predictive bridge maintenance and propose integrating robotics with vision solutions. Nguyen et al. [5] present the development of a Building Information Modeling (BIM)-based Mixed Reality (MR) application to enable and enhance the process of managing bridge inspection and maintenance tasks remotely from the office. Gaspari et al. [6] present a study comparing two methodologies for bridge inspection. The first approach combines traditional topographic and GNSS techniques with TLS and photogrammetry, using cameras mounted on UAVs. Although this method produced a highly accurate model with centimetric precision, it was time-consuming. In contrast, the second method involving UAV-mounted LiDAR is a valid alternative for measuring bridges with moderate accuracy (5–10 cm). Owerko and Owerko [7] present a novel approach to inspections of as-built reinforcement in incrementally launched bridges by modified photogrammetry and High-Definition Surveying—a combination of terrestrial laser scanning, computer technology, and precision control networks. A review of methods for Remote and Autonomous Bridge Inspection with accuracy was presented by Rakoczy et al. in [8].

Hines et al. [9] present an overview of technologies for measuring distances or object dimensions available in the AEC/FM (Architecture, Engineering, Construction, and Facility Management) domain. This overview is divided into three main categories: micro-scale, average, and large-scale measurements. Various measurement technologies with different sophistication levels are presented, from measuring tapes to surveying tools (total stations), ultrasound devices, laser measurers, laser scanners, or computer vision-based technologies (photogrammetry/videogrammetry).

According to Scherer and Lerma [10], surveying technology related to total stations (TSs) has changed revolutionarily in the last fifty years. The steps initiated by TS manufacturers seem to be going in the right direction. However, more integration among surveying, spatial geodesy, and photogrammetry is required to provide high-end technology for future generations.

This paper presents an attempt to use a Scanning Total Station (STS) and photogrammetric documentation recorded with the use of an Unmanned Aerial Vehicle (UAV) for the inspection and inventorying of the dimensions of a bridge. The research goal of the project was to analyze the possibilities of the integration of data from the STS and UAV, considering the obtained accuracies and assuming the use of commonly used equipment—in the mid-price class. The fusion of STS and UAV data is applied to the case study of a truss railway bridge over the Vistula River in Poland.

2. Methods of Remote Bridge Inspection and Used Equipment

The visual remote inspection and the geometry inventory of bridges with the use of STS and UAVs are presented separately in two sections. The applied software is presented in one section. The possibilities of integrating data from these two methods are presented in the next section, and then tested on the example of experimental studies of a truss bridge.

2.1. STS Applications for Bridge Inspection and Inventory

2.1.1. Surveying Equipment

The STS can be used in various SHM applications. For example, Omidalizarandi et al. [11] and Erhart et al. [12] present applications for vision-based displacement and vibration analysis of bridges. Sanchez-Cuevas et al. [13] present the application of the STS to assist UAVs in inspection, which requires physical contact between the aerial platform and the bridge surfaces without compromising the propellers, e.g., beam deflection analysis or measuring crack depth with an ultrasonic sensor.

In the case study presented in this manuscript, the geometry of the selected bridge part was measured using the Leica Nova MS50 MultiStation, Leica Geosystems, Heerbrugg St. Gallen, Switzerland (STS). This device can conduct precise reflectorless measurements and has the ability to create point clouds by laser scanning. The basic parameters of this device are an angular accuracy of 1″, a distance measurement accuracy onto a prism of

1 mm + 1.5 ppm and onto any surface of 2 mm + 2 ppm, scanning with 1000 Hz mode—to a range of 300 m with range noise of 1.0 mm at 50 m and scanning with 1 Hz mode—to a range of 1000 m with range noise of 0.6 mm at 50 m (Grimm [14]). For better presentation, when changing the distance from 20 m to 500 m, the accuracy of direct measurement changes from 1.0 mm to 1.8 mm (with reflectors) and from 2.0 mm to 3.00 mm (without reflectors). Before use in the field, the accuracy of the measurements was tested under controlled conditions—Olaszek et al. [15].

2.1.2. Direct Dimension Measurement Obtained Accuracy Using TS

Most of the TS applications presented in existing publications concern displacement monitoring where reflectors (prisms) are primarily used—for example, Alade [16], Onu [17], Liu et al. [18]. Zeidan et al. [19] investigated the accuracy of reflectorless total station observations during the process of monitoring and setting out engineering structures. The accuracy of reflectorless TS observation depends mainly on the signal power, which is reflected from the reflecting surface. The intensity of the returning signal depends on the distance from the TS and the reflectivity of reflecting surfaces of different colors and made of various materials.

Due to the remote nature of the measurements, this research focuses on reflectorless measurements. Initially, laboratory tests were carried out to assess the accuracy of the measurement method in various environmental conditions. The tests aimed to measure the dimensions of the beam using reflectorless measurements and point cloud scanning and then comparing the results with the known dimensions of the beam—Olaszek et al. [15]. The laboratory test was also performed to stimulate the conditions that prevail during field tests, mainly the distance between the station, the measured elements (about 14 m), and the horizontal viewing angle (about 60^g). The errors of the direct reflectorless measurement of the element dimensions were below 2.4 mm.

In the case of measuring permanent deformations of a superstructure or settlements above piers or abutments, remote and periodic measurement using TS is only possible if prisms had been previously installed in the middle of the spans and above the piers and abutments. It should be noted that using reflectorless measurement does not ensure proper measurement accuracies in that case.

2.1.3. Dimension Analysis Based on the Scanned Point Cloud and the Obtained Accuracies

The idea of point cloud measurements is to obtain a large quantity of adequately accurate data. The accuracy of each obtained point is usually lower than when conducting prism-based measurements. Point clouds created in this way are well suited to general assessments of the shape or main dimensions of large objects. Data processing is required to achieve more accurate results. In the case of steel structures, the measured shapes are often geometrically complicated due to the many detailed connections. Additionally, in the presented case study, the final point cloud was collected using multiple different measurements, which further decreased the accuracy of each point measured.

The STS device used in the tests has the ability to collect many millions of points in a single point cloud. Such large quantities of data must be evaluated and processed to achieve the desired accuracy. Many different tools and approaches are often used to determine which points are useful and which are not (outliers). Point clouds collected in these tests were simply put through a statistical outlier removal (SOR) process. The remaining data were then further reduced to only contain the relevant parts of the point cloud (cropping). The remaining points represent the shape of the objects; however, there is no easy way to obtain accurate measurements. A geometrical model is proposed to mitigate the lack of accuracy of individual points.

Many steel structural elements can be idealized as composed of plane. Some of these planes are parallel, such as in the case of a rectangular beam, which consists of two sets of parallel planes (the sides). The proposed idea was to use the obtained points and fit them to a geometrical model of sets of parallel planes. This approach is not yet universal; however,

it can be very useful in many engineering applications. The fitting of sets of points to geometrical models is a broad topic with many possible solutions. Two approaches are proposed and presented in Figure 1.
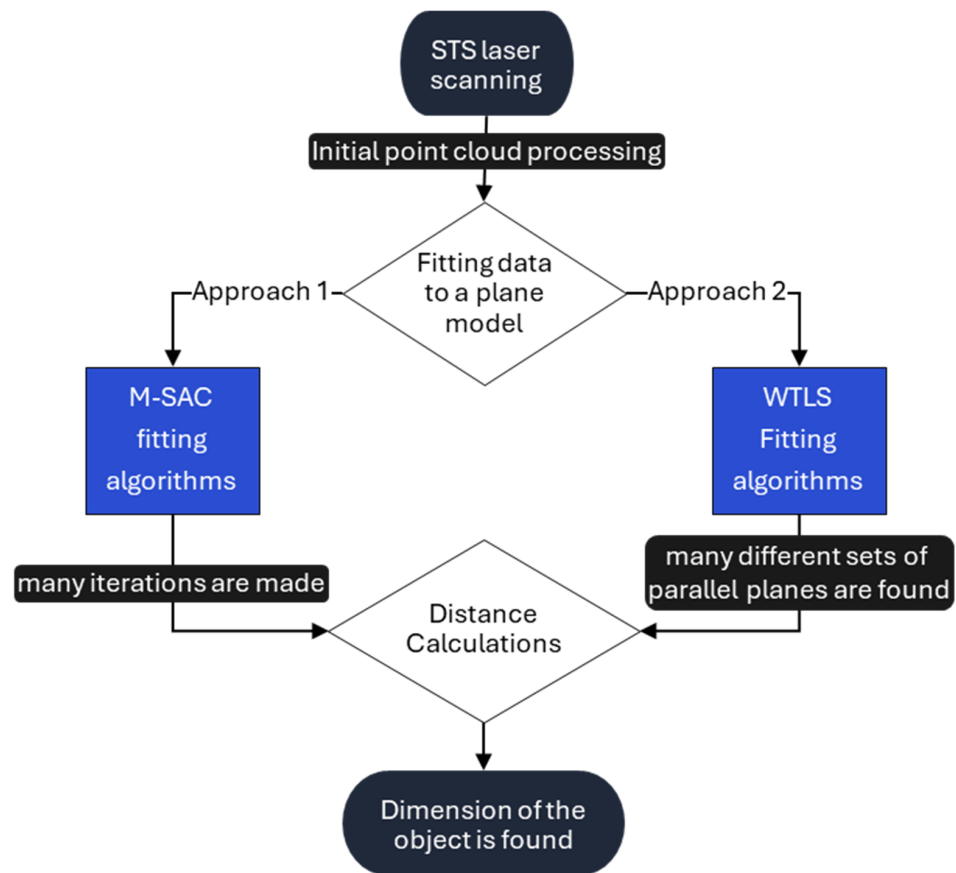

Figure 1. Applied algorithms for determining dimensions from the point cloud calculations.

The first approach uses a modified version of the random sample consensus algorithm (RANSAC) and an M-estimator function called M-SAC. The first step is to find an initial plane by specifying the direction of a normal vector of a plane. This vector is used next to see the first best-fitting plane. In this case, the angle tolerance of the normal plane can be relatively high, as only the first plane in a general direction has to be fitted. After fitting one plane to a subset of points in the point cloud, the algorithm uses its normal vector to fit any other plane within a certain angular tolerance. The result is two planes with normal vectors within a tolerance set to 0.05^g. Due to the nature of RANSAC, the resulting planes will differ in each iteration of the algorithm. The algorithm is repeated many times (1000 at minimum) to achieve more accurate results. The distance between the planes is calculated as the distance between their centroids, as the planes are not geometrically parallel.

The second approach is to use a Weighted Total Least Squares (WTLS) algorithm as proposed by Shakarji et al. [20]. This algorithm finds the best-fitting set of parallel planes from the collection of supplied points. The fitted planes are always parallel, as there is no tolerance between their normal vectors. Weighted centroids of two sets of data points corresponding to two parallel planes were found. Then, a single normal unit vector was found by utilizing least squares minimization. This vector is the normal vector of a set of parallel planes. Accuracy, in this case, is not determined by tolerances or chance but by the initial set of points selected. Many different sets are used. The initial sets of points can be found by selecting them by hand (visually) or by using similar algorithms as in the first approach. The distance can be directly calculated as the distance between two parallel planes.

The errors of dimensional analysis on the basis of the scanned point cloud, determined during the laboratory tests described above, were below 3.5 mm for the point cloud data mean distance algorithm and below 4.2 mm for the plane fitting algorithm—Olaszek et al. [15].

2.1.4. Restrictions on the Use of STS

Reflectorless (prismless) technology is practical for remote measurements but has some limitations. According to Fawzy [21], the accuracy of the measured distance using the reflectorless TS option and the prismatic option converge for short distances (up to 35 m). Above this distance, the accuracy of the measured distance by the prismatic option is better than the accuracy by the reflectorless option. The increasing inclination angle for the reflecting surface leads to an increase in the error of the distance measured by the reflectorless TS, and the maximum accuracy is to be obtained when the inclination angle for the target is kept equal to zero. Furthermore, according to Haddad and Ishakat [22], laser scanning accuracy cannot reach the accuracy of geodetic instruments and cannot provide the possibility of increasing accuracy through larger image scales.

Additionally, due to the relatively long scanning time compared to classic geodetic measurements, it is much more difficult to scan when forced and free vibrations occur in the operated object.

2.2. UAV Applications for Bridge Inspection and Inventory

2.2.1. Equipment

The aerial remote system comprises a low-cost UAV manufactured by DJI Shenzhen, China, specifically the Mavic Mini 1 model. This UAV has a maximum take-off weight of 249 g, a maximum flight speed of 13 m/s, and a maximum transmission distance of 4000 m in an unobstructed and interference-free environment. With a maximum flight range of 30 min per battery set, it offers considerable operational endurance. The drone features a geodesic GNSS system with a hovering accuracy range of ± 0.5 m vertically and ± 1.5 m horizontally, complemented by an internal inertial measurement system for stabilization. Additionally, it is equipped with a native camera mounted on a suspension/pivot system known as a gimbal, incorporating internal stabilizers. The camera is equipped with a 1/2.3″ CMOS sensor (6.17 $\times$ 4.55 mm) capable of capturing images with resolutions of up to 12 MP (4000 $\times$ 3000) and a focal length of 4.25 mm.

The adoption of commercial drones in the Architecture, Engineering, and Construction (AEC) industry has seen rapid growth. Notably, Nwaogu et al. [23] highlight their increasing use, particularly in structural health monitoring applications for bridges. For instance, Ribeiro et al. [4] discuss leveraging UAVs for the remote inspection and monitoring of civil engineering structures. They present a case where the same UAV model is utilized to create orthophoto mosaics of degraded regions, showcasing exposed steel rebars within an industrial building. Similarly, Montes et al. [24] have applied the Mavic Mini UAV model and proposed an enhanced visual inspection framework. This framework enhances the visualization of bridges and facilitates the monitoring of deterioration changes through periodic inspections. By generating multiple 3D models of a bridge over time, this approach enables engineers to assess the bridge's technical condition and track inspection progress with accuracy, effectively serving as time capsules of its physical state.

2.2.2. Photo Analysis Algorithms Used and Obtained Accuracies

A photography, in contrast to laser scanning, is a passive vision system, necessitating specific processing steps to derive point clouds [1] and acquire dimensions in 2D. Figure 2 illustrates this workflow. The algorithms utilized for extracting point clouds from images include Structure from Motion (SfM) and Multi-View Stereo (MVS) [25].
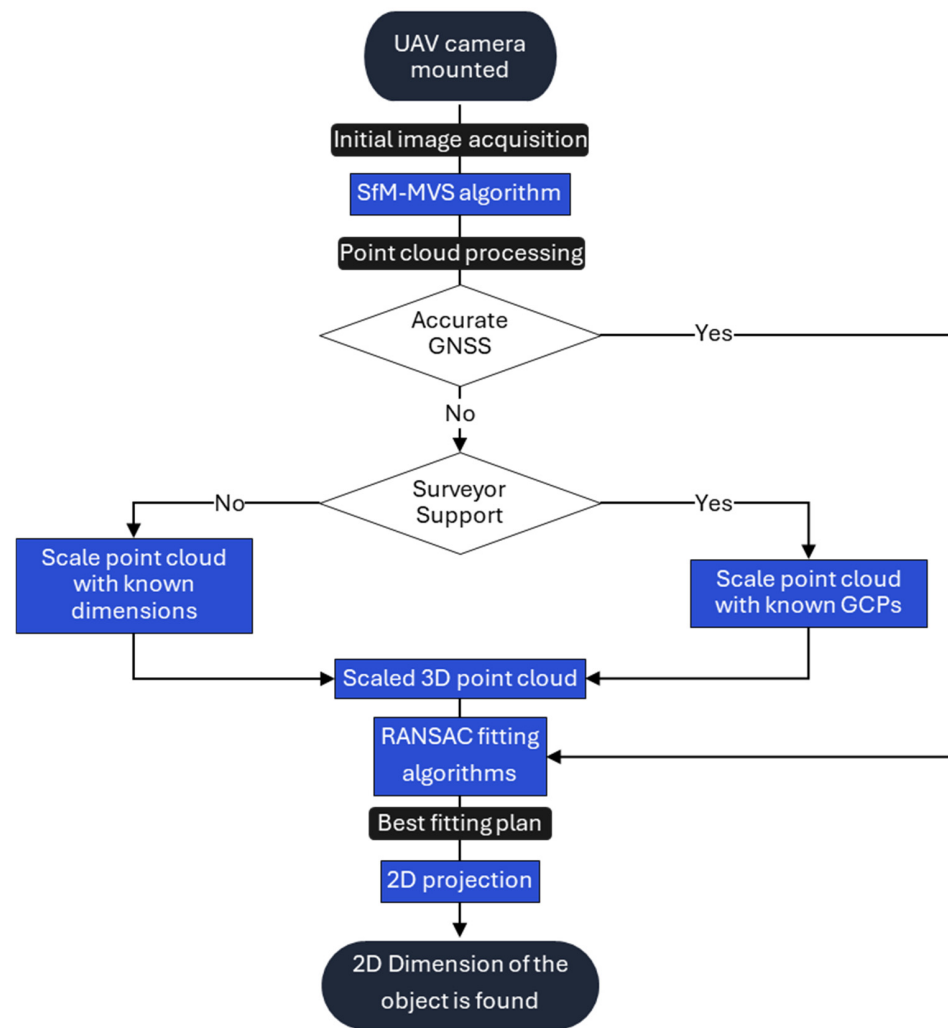
Figure 2. The applied algorithms for determining dimensions from the photogrammetry calculations.

SfM operates by analyzing the geometric structure of a scene from multiple images taken from various viewpoints, enabling the estimation of the camera's location and orientation relative to the scene. This analytical process performs the reconstruction of 3D models in sparse point clouds. In contrast, MVS complements SfM by correlating corresponding points in multiple images to generate dense 3D reconstructions with high accuracy and detail, thereby refining the estimation of location and orientation.

Centimeter-level accuracy is achieved by maintaining a low Ground Sampling Distance (GSD) value. GSD represents the ratio between a real-world measurement and the pixel size, which is directly proportional to the distance from the target. Equation (1) is used to compute the GSD.

$$GSD = \frac{D}{f} \cdot \frac{S_w}{I_w} \tag{1}$$

where GSD is expressed in cm/pixel, D is the flight distance from the target in cm, f is the focal length of the camera in mm, S_w is the sensor width in mm, and I_w is the image width in pixels.

Whether the resulting point cloud is scaled depends on the presence of georeferenced coordinates in the images captured by the UAV. If coordinates are unavailable, processing relies on previously known dimensions or assistance from a surveyor to extract Ground Control Points (GCPs). In cases where known dimensions are accessible, the scaling of the point cloud is achieved using one or more known values. Alternatively, if a surveyor provides GCPs, the point cloud is georeferenced to a specified reference system [4].

Subsequently, within the scaled point cloud, the Random Sample Consensus (RANSAC) algorithm is employed to identify the best-fitting plane among the points [26]. Afterward, the reference system is aligned with the identified plane, and the depth dimension, representing the distance of points from the plane, is removed, ensuring that all points lie within the 2D plane. As a result, a contour of the flattened point cloud is generated, facilitating the determination of the 2D dimensions of the component under analysis.

2.2.3. Restrictions on the Use of UAVs

The utilization of Unmanned Aerial Vehicles (UAVs) is subject to various limitations and regulations, particularly as they operate within aerial spaces. Adherence to these regulations is crucial, with careful consideration of authorizations being imperative. In Poland, compliance with regulations established by the Civil Aviation Authority (CAA) and the European Authority for Aviation Safety (EASA) is mandatory, a requirement that was fully met during the campaign.

In addition to regulatory compliance, it is crucial to acknowledge specific hardware limitations relevant to the actual UAV employed in this campaign and its intended applications. The lightweight design of the equipment presents a notable challenge, particularly in windy environments, where it may experience instability issues during flight. Moreover, operational constraints were encountered regarding the camera angle throughout operations, limiting its ability to capture images directly above the UAV.

Furthermore, the drone faced disruptions due to the magnetic field surrounding such a large metallic mass as the railway bridge. These disruptions notably affected the accuracy of delicate sensors such as the compass and GNSS (Global Navigation Satellite System), hindering the seamless integration of GNSS information into the processing workflow. Additionally, special attention must be paid to the maximum flight duration to ensure operational safety and efficiency.

Given these challenges, it is imperative to implement thoughtful mitigation strategies and operational protocols during UAV operations to address and effectively overcome these obstacles.

2.3. Software

In this study, several software tools were used for data processing and analysis. Cloud-Compare v2.13.2 [27], an open-source software for 3D point cloud processing, was used for data manipulation (e.g., converting from 3D to 2D), visualization, and comparison. Leica Cyclone v.9.1 [28] was employed for managing and visualizing data captured by Leica's scanning equipment. To create the reality model based on photogrammetry, iTwin® v1.1.394 [29] was employed. To convert the reality capture data into 3D models, Autodesk ReCap v.2022 [30] was used, as was MathWorks MATLAB v.R2022a [31] for the implementation of fitting data algorithms. For precise 2D and 3D design, drafting and detailing, Autodesk AutoCAD v.2022 [32] was utilized. All these software tools were used for comprehensive analysis and integration of the remote inspection data presented in this paper.

2.4. Integrating Data from STS and UAV Methods

The possibility of integrating data from STS and UAV methods depends on the STS's localization capabilities. The convenience of locating the STS can be determined by the distance d_{rs} of the station from the tested bridge element and the inclination α_{rs} of the reflecting surface of this element in relation to the plane perpendicular to the target axis. In the case of reflectorless STS measurements, it is recommended that the distance limit d_{rs_lim} and the reflecting plane tilt angle limit α_{rs_lim} are not exceeded. Figure 3 shows the scope of STS and UAV application, taking into account the areas of recommended independent use of individual methods and the recommended area of mutual validation of measurement results. The proposed diagram should be used when selecting STS or UAV methods separately for each bridge element or global dimension.
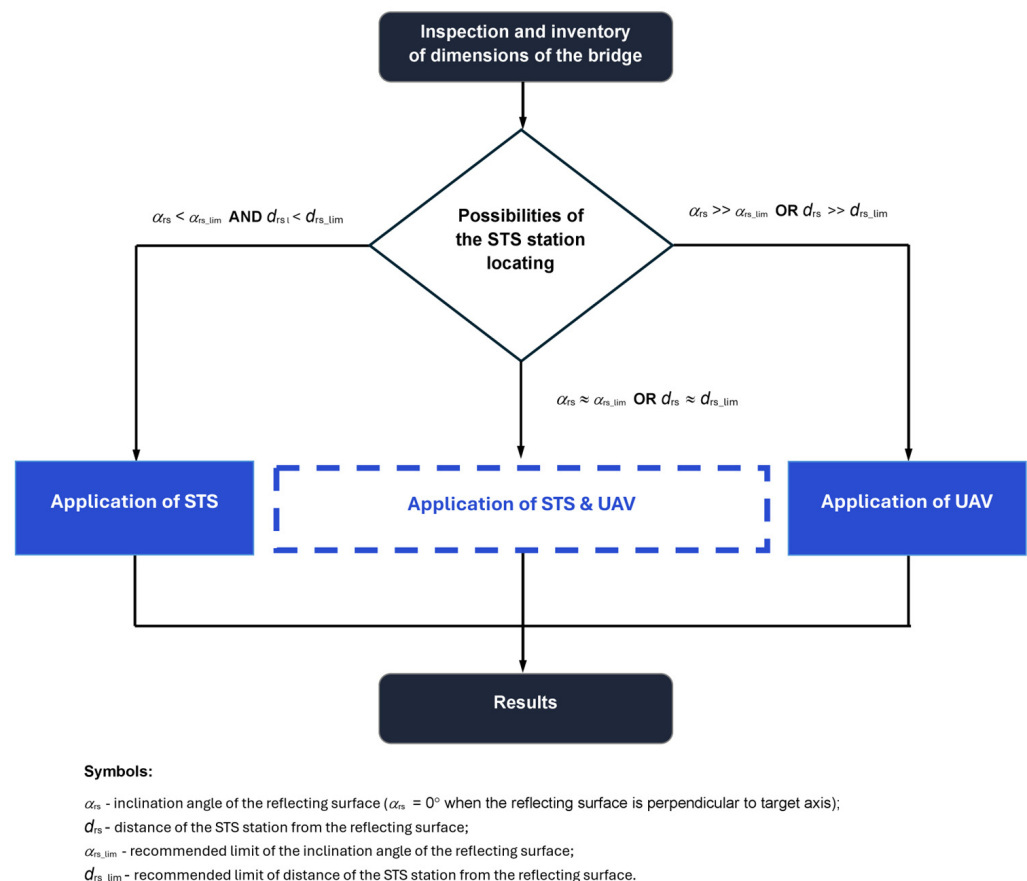
Figure 3. The possibilities of integrating data from STS and UAV methods.

In the case of the STS used during this research, the ranges depend on the reflecting surfaces; according to the documentation [14], a distance limit of d_{rs_lim} 2000 m can be assumed. According to the authors' experiences, the angle α_{rs} should not exceed $45°$.

3. Materials—Bridge Selected for Verification Tests

Verification tests were conducted on a multi-span, steel truss railway bridge (Figure 4). The bridge is located in Warsaw over the Vistula River. The river is almost 400 m wide. The bridge has two separate structures for each of the railway lines. One of these structures was constructed in the 1980s and was renovated in 2015; the second was rebuilt in 2015. Each of the structures consists of seven spans of over 66 m in length and two smaller spans at each end.

The experiment consisted of two parts related to two types of measurements:

- The selected basic dimensions of the span structure, i.e., the span length, height, and width of the truss and the length of the selected diagonal and post components.
- The selected dimensions of one main structural connection of the truss.

A truss span over the riverbank was selected for the experiment (Figure 5).

Selected basic dimensions of the bridge span are shown in Figure 6. The STS measurements were carried out from three positions: one for the span length and two for other measurements. The distance between the station and the measured elements was about 65.0 m and 16.4 m for the span length measurement and from 15.0 m to 23.3 m for the other measurements. The horizontal angle for the span dimension measurements was 11.03^g and 210.95^g, respectively, and for the other dimensions it was 175.17^g and 156.04^g. The vertical angle was 96.09^g and 84.90^g for the span measurements and 71.04^g and 72.70^g for the others. The span dimension was calculated by measuring the edge of the top of the bearing (T-shaped washers) and dividing their length in half to obtain the center distance.

The rest of the dimensions were directly measured through two characteristic points. The image acquisition with the use of the UAV was carried out from the smallest possible safe flight distance, certifying a GSD of 0.18 cm/px (about 5 m from the structure).

(a)

(b)

(c)

Figure 4. Bridge selected for verification tests: (**a**) satellite image with selected bridge highlighted—Google Maps; (**b**) view of the truss spans over the river; (**c**) view from the side of the truss spans over the road.
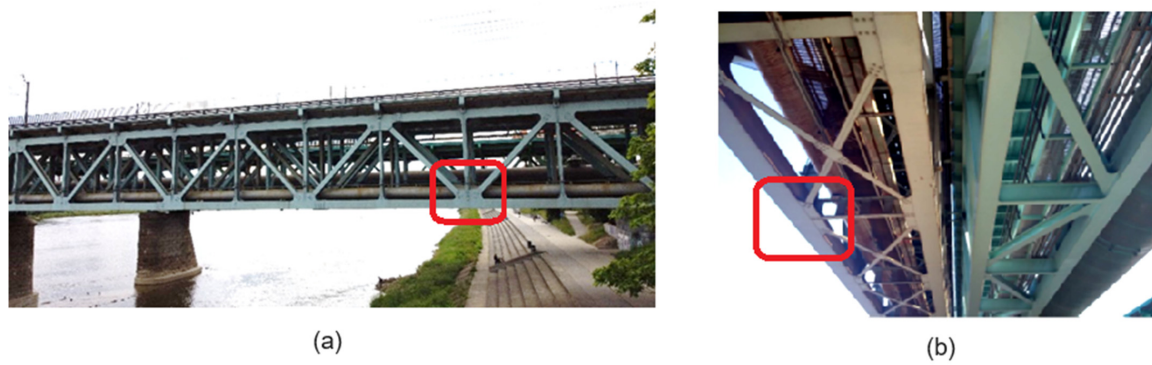
Figure 5. Views from the riverbank of the span selected for the experiment with the analyzed connection marked: (**a**) side view; (**b**) view from below.
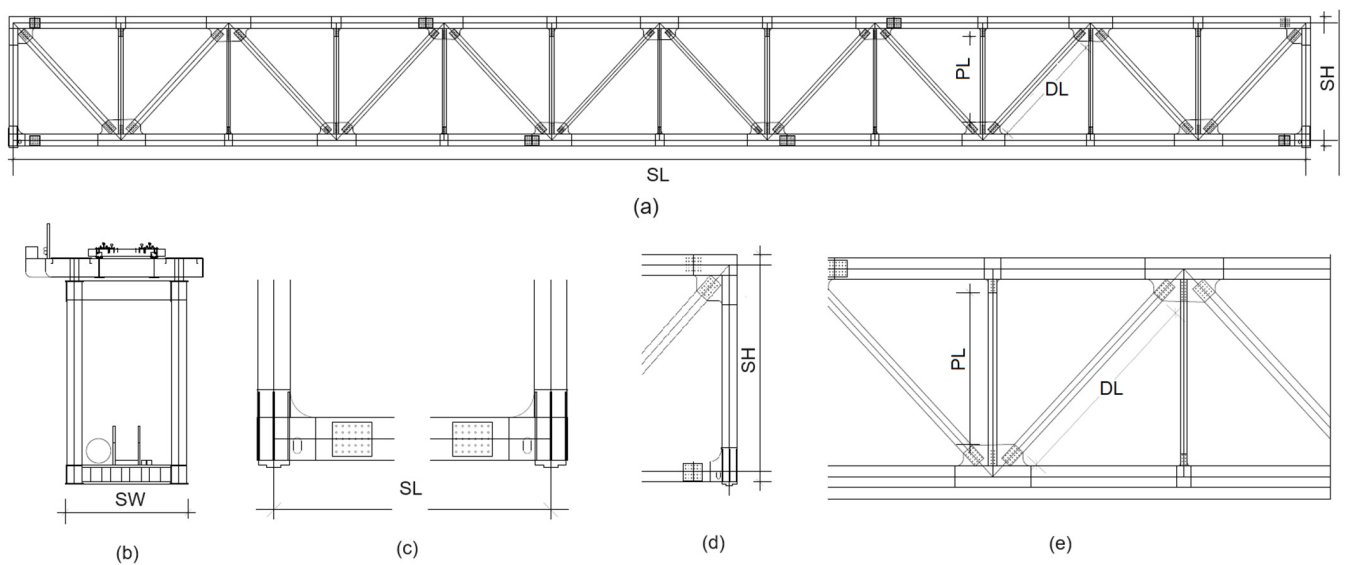
Figure 6. Part of the documentation drawings of the span showing the selected basic dimensions: (**a**) the longitudinal section and enlargements; (**b**) cross-section with the span width marked—SW; (**c**) the start and end points of the span length measurement—(SL); (**d**) the span height marked—SH; (**e**) the diagonal length—DL—and the post length—PL—marked.

One main structural connection, shown in Figure 3, was selected for the second part of the experiment. It is a W-type asymmetrical connection, joining one vertical member and two diagonal members with the lower chord of the truss. The members are connected using rivets and a gusset plate. Each of the three riveted connections is unique in the number and position of the connectors. Selected local dimensions for the measurements of the connection are shown in Figure 7.

This connection was selected for remote inventory and inspection using STS and UAV since it was designated as repaired in the post-renovation documentation. In addition, the location of the connection provided good access for the measurements from the sidewalk under the bridge.

The measurements using STS were carried out from two positions. The distances between the station and the measured elements were about 16 m and 22 m, and the viewing horizontal angles were about 75^g and 85^g, respectively. Concerning the image acquisition from the UAV platform, the nearest position ensuring flight safety and centimeter-level accuracy was chosen, ensuring a GSD of 0.18 cm/px (frontal view at about 5 m from the structure).

It is important to note that the measurements were taken on different days, although they were conducted within close temporal proximity and around the same time of day. The

weather conditions were similar during both measurement sessions. Thus, the authors do not believe that any large differences in the data can be attributed to the thermal expansion or contraction of the bridge.

(a)
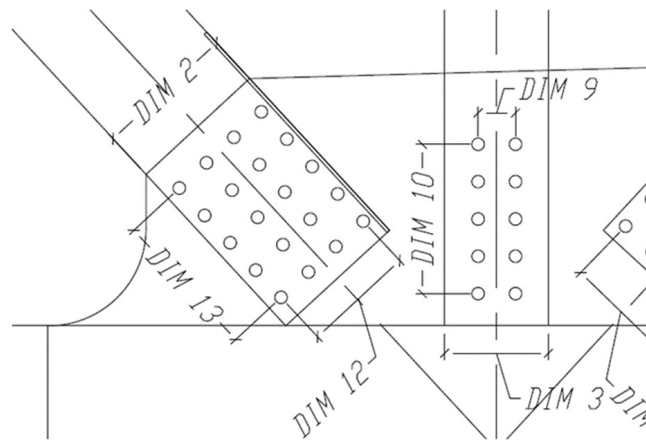
(b)

Figure 7. The main truss connection: (**a**) a close-up view and (**b**) part of the documentation drawing of the connection showing the selected dimensions.

Figure 8 presents photographs of the analyzed connection taken using the UAV and the STS.

(a)

(b)

Figure 8. Photographs of the analyzed connection: (**a**) taken from a UAV; (**b**) taken from the STS.

4. Results and Analysis

This section demonstrates the results and discussion of the measurements performed on the bridge span using two methods: Scanning Total Station (STS) and Unmanned Aerial Vehicle (UAV). The compatibility of the measurements is evaluated by comparing the results with the design documentation, and the relative differences (RDs) are analyzed to assess the performance of both techniques.

4.1. Basic Dimension Measurement Results

The results of the measurements of the basic dimensions of the bridge span with the use of STS and UAV are presented in Table 1. The resulting dimensions are compared to the dimensions from the technical documentation.

Table 1. The results of measurements of the basic dimensions using the STS and UAV and data from the documentation (dimension markings from Figure 4).

Dimension	Documentation X_d [mm]	Measurement X_m [mm]		Relative Difference RD	
		STS	UAV	STS	UAV
Span Length—**SL**	66,000	65,979	65,279	−0.03%	−1.09%
Span Height—**SH**	6570	6572	5969	0.03%	−9.15%
Span Width—**SW**	4010	4018	---	0.20%	---
Diagonal Length—**DL**	5916	5883	6024	−0.56%	1.83%
Post Length—**PL**	4373	4277	4259	−2.20%	−2.61%

The RD was calculated as the difference between the measured value X_m and the value (Absolute Differences—ADs) from the design documentation X_d divided by the dimension from the design X_d:

$$RD = \frac{AD}{X_d} = \frac{(X_m - X_d)}{X_d} \tag{2}$$

where X_m is the result of measurements using the STS or UAV.

4.2. Analysis of Basic Dimension Measurements

For measurements using the STS, the relative difference with the documentation was below 2.2%—the highest compliance for span length, height, and width (below 0.2)%. The Absolute Differences were 21 mm for the span length, 2 mm for the height, and 8 mm for the width. Such deviations are in accordance with the old Polish standards as well as the current European ones—Băncilă et al. [33]. Greater differences were obtained when measuring the post and the diagonal length: from −2.20% to −0.56% (from 96 to 33 mm). Such deviations most likely result from the adopted (the only visible) points defining the dimensions of the diagonal and the post length when measuring with the STS (Figure 9).

The smaller measured values may be due to the excess dimensions of the gusset plate originally reported in the documentation. Such measurement results do not indicate the lower accuracy of the STS in this case, but only that the method of assuming the beginning and end of the element is inconsistent with the documentation.

The UAV captured 646 images of the bridge span, which were processed using photogrammetry to create a point cloud. This method enabled the creation of a digital model of the span, which was analyzed using iTwin® v1.1.394 software (Figure 10). The strategy outlined in Section 2.2.2 for determining dimensions from the photogrammetry calculations was then applied. However, several limitations were identified, including magnetic fields surrounding the large metallic structure that interfered with the inertial sensors, as well as an insufficient number of images in specific areas, resulting in voids or gaps in the point cloud. Additionally, during this campaign, there was no surveyor support with GCPs over the structure. Nevertheless, the point cloud was scaled based on known dimensions, such as the distance between two posts.
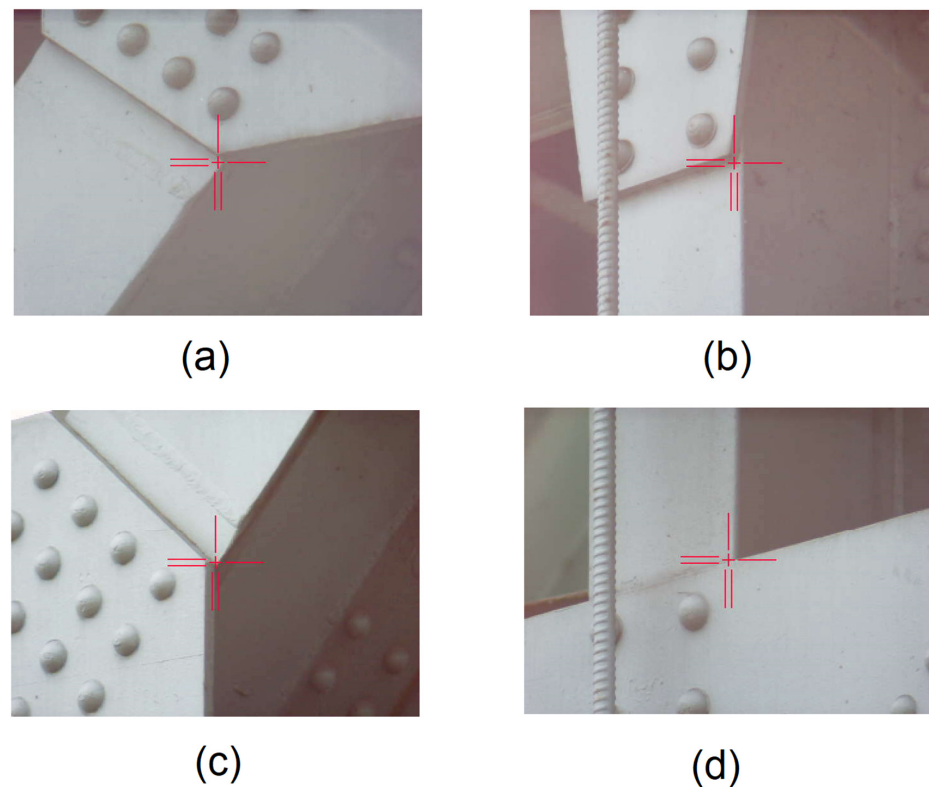
Figure 9. Measuring the diagonal and post length with the STS; points defining the dimensions were marked automatically with a red cross: (**a**) the top of the diagonal; (**b**) the top of the post; (**c**) the bottom of the diagonal; (**d**) the bottom of the post.

Figure 10. Photogrammetry of the inspected bridge span.

For measurements using the UAV, the relative difference with the documentation was below 2.61% for span length and for diagonal and post length. The greater Absolute Difference was 9.15% for the span height. However, it was not possible to gather data on the span width, as only images of the façade were captured. The greater Absolute Differences were 721 mm for the span length and 601 mm for the span height. The smaller Absolute Differences were 114 mm for post length and 108 mm for diagonal length.

Differences between measurements using the UAV and STS were also calculated. In the case of span length measurements, the difference was −700 mm, and for height, it was −603 mm; in the case of the diagonal length it was 140 mm, and for post length it was −18 mm. In these measurements, the STS measurements should be considered more accurate. The estimated accuracy (measurement uncertainty with a 95% probability) of the

direct measurement using the STS was about ± 5 mm for the span length and ± 3 mm for the span height.

This analysis highlights the UAV's effectiveness for remote measurements but also reveals limitations in capturing certain dimensions in non-georeferenced models and ensuring full coverage of the structure.

4.3. Detailed Dimension Measurement Results

The W-type connection previously highlighted was measured using STS and UAV systems to perform remote inventory and inspection. The survey aimed to compare the available design documentation of the selected connection with survey data. The only available documentation was made during renovation works. No original design documents could be found.

The STS was used to create a combined point cloud of the whole connection. Additionally, reflectorless measurements were also performed. During the scanning process, three distinctive point clouds were created, one from each measuring station. Two of the point clouds were captured from the front of the gusset plate and one from below the structure of the truss. Two of the three point clouds were used in calculations and dimension comparisons. These point clouds consist of 602,158 and 611,099 points, respectively. The first cloud has a mean Gaussian volume density of 13.5 p/cm^3 (points per cubic centimeter) with a standard deviation of 2.7 p/cm^3 calculated with a spherical radius of 1 cm and a mean surface density of 18.1 p/cm^2 with a standard deviation of 3.6 p/cm^2. The second cloud has a mean volume density of 16.2 p/cm^3 with a 3.0 p/cm^3 standard deviation and a mean surface density of 21.6 p/cm^2 with a standard deviation of 4.0 p/cm^2. Only the main elements of the connection were needed for calculations and verification of dimensions. All unnecessary parts captured by the STS device were cropped out. The STS device was set to a resolution of 0.0079^{g} for both vertical and horizontal angles. The maximum capture distance was set to 16.5 m and the minimum measured distance was 15.06 m. The first point cloud captured a wider area, while the second was more focused on the gusset plate.

Finally, the resulting point cloud from both systems required some processing techniques to be comparable to the available 2D drawings. Flattening algorithms were used. Firstly, a best-fitting plane was found, and then the dataset points were all projected onto the plane as shown in Figure 11. The projected points were then traced to create a contour of the flattened point cloud.
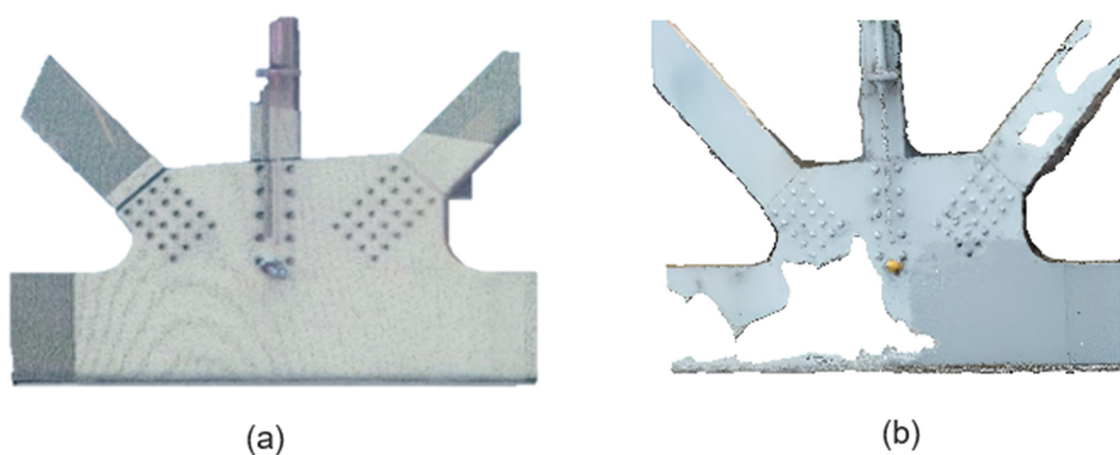

(a)   (b)

Figure 11. A point cloud of the analyzed connection projected onto the 2D plane: (**a**) the STS system calculation; (**b**) the UAV system calculation.

The resulting dimensions obtained from the STS and UAV are also compared to the dimensions from the documentation and presented in Table 2. The relative deviation (*RD*) of the basic dimensions was calculated according to Equation (1).

Table 2. The results of measurements of the connection using the STS and UAV and data from the documentation (dimension markings from Figure 7).

Dimension	Documentation X_d [mm]	Measurement X_m [mm]		Relative Difference *RD*	
		STS	UAV	STS	UAV
DIM 9	90	153	143	70.00%	58.89%
DIM 10	360	506	495	40.56%	37.50%
DIM 12	270	259	260	−4.07%	−3.70%
DIM 13	360	341	338	−5.28%	−6.11%

4.4. Analysis of Detailed Dimension Measurements

The final comparison of the STS and UAV systems is presented in Figure 12. Several discrepancies between the documentation and the observed structure were found during surveying. For example, the left diagonal member is connected with a smaller gusset plate than indicated in the drawings. The shape of the gusset plate on the left side seems to have been altered.
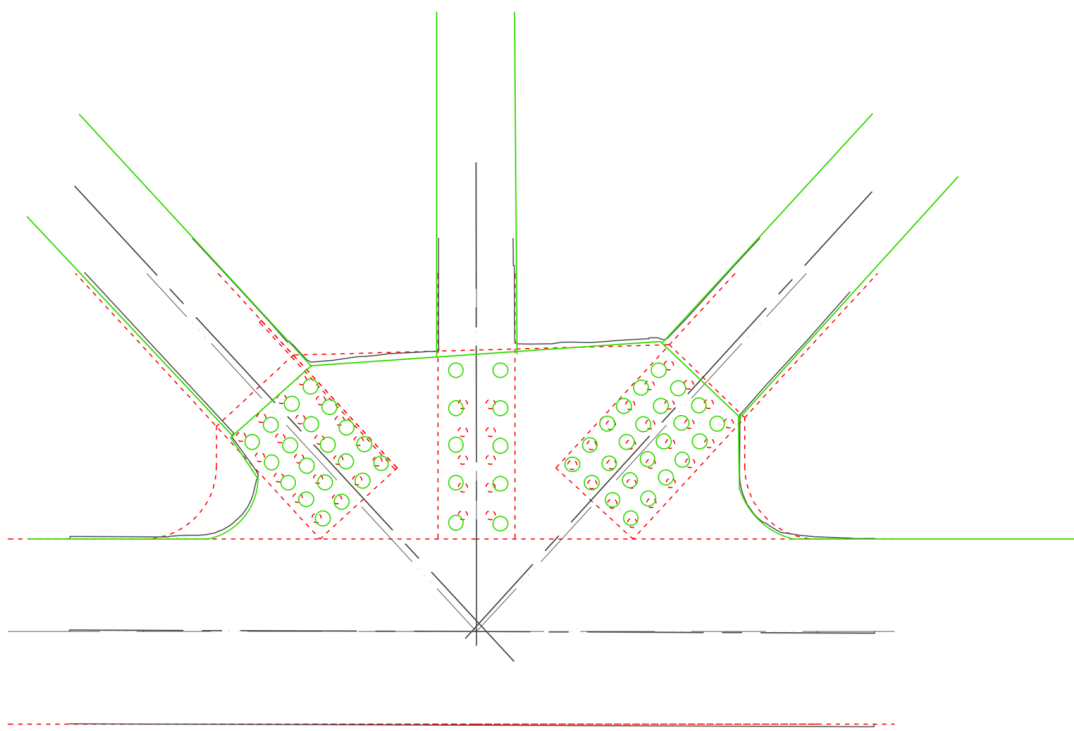
Figure 12. Geometry verification: STS point cloud contour (black solid line), UAV point cloud contour (green solid line), and documentation drawing (red dotted line).

It was discovered that the rows of rivets connecting the vertical member are spaced horizontally (DIM 9) with a 70.00% and 58.89% relative deviation and vertically (DIM 10) at a 40.56% and 37.50% relative deviation for the STS and UAV system, respectively, compared to the dimensions from the documentation. The rest of the dimensions, such as the member width, the height of the lower chord, or the spacing (between DIM 12 and 13) of the diagonal member's connectors, were measured as −4.07% and −3.70% of relative deviation (DIM 12) and as −5.28% and −6.11% of relative deviation (DIM 13) for the STS and UAV system, respectively, compared to the dimensions from the documentation.

In this case, the differences between measurements using the UAV and STS were much smaller than in the case of measuring the basic dimensions of the span. In the case of rivet location measurements DIM 9 and DIM 10, the difference was between −10 and −11 mm, and in DIM 12 and DIM 13, the difference was between −3 and 1 mm. The estimated

accuracy (measurement uncertainty with a 95% probability) of the direct measurement using the STS was about ±2 mm for the measurements of the connection dimensions.

Based on photos taken by the UAV, it was found that similar discrepancies between the available pre-renovation documentation and the existing structure also occur in other connections of this span. This is presented in Figure 13. Such discrepancies might be related to changes made during the construction process, which were not included in the pre-renovation documentation.
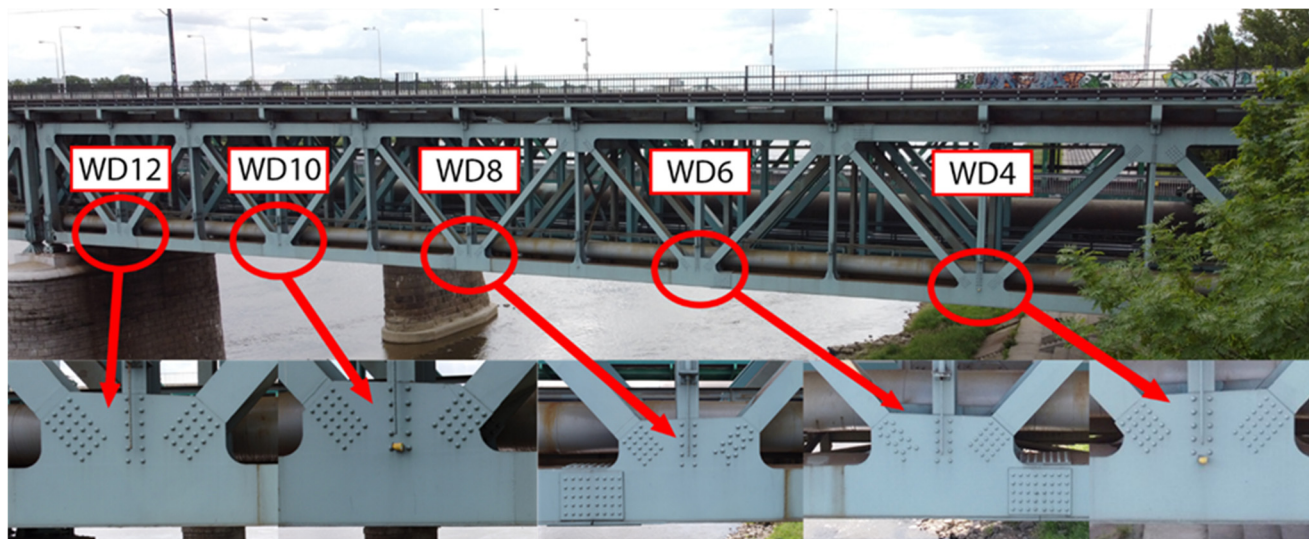
Figure 13. The occurrence of an analyzed discrepancy between the documentation and the observed structure in other connections of the span (based on photos taken by the UAV).

5. Conclusions

This study highlights the effectiveness of the STS and UAV systems in the remote inspection and geometrical inventorying of bridge structures. Each method presents distinct advantages and limitations, but their integration offers promising potential for comprehensive, cost-effective, and non-invasive structural monitoring. The presented proposal for remote inspection using more suitable equipment and a robust data processing technique can produce results comparable to those of classical inspection. As can be summarized, remote methods in most cases allow for measurement with accuracies only two times less than classic touch-based methods. That means the value of error is two times bigger. This applies to measurements carried out using the total station with and without reflectors. In the case of UAV use, the errors may be even greater, but these are high accuracies useful for most applications in bridge inspection.

This research confirms that the STS provides high accuracy in direct measurements of bridge dimensions, with deviations from the reference documentation within acceptable engineering tolerances (below a few mm). Specifically, the reflectorless measurements achieved errors below 2.4 mm in laboratory settings. The point cloud data produced by the STS was also used for more complex geometrical analyses, such as fitting surfaces to planes, although with slightly higher deviations.

On the other hand, UAV-based photogrammetry, while slightly less precise than STS, provided considerable advantages in terms of coverage and efficiency. The UAV system enabled the creation of a detailed point cloud for a large section of the bridge, achieving over 90% compliance with reference dimensions. This level of accuracy is adequate for many remote inspection applications, particularly for identifying large-scale structural anomalies. However, UAVs faced challenges in capturing certain critical dimensions, such as span width, due to voids in the point cloud caused by an insufficient number of images. Furthermore, external factors like wind, battery duration, and interference from the bridge's metallic structure introduced variability in the quality of the data collected by the UAV.

One of the key findings of this research is the potential for integrating STS and UAV systems to overcome the individual limitations of each technology. While STS excels in precision, UAVs can quickly cover large areas that are difficult to reach, such as high bridge spans or inaccessible connections. Combining the point cloud data from both systems can provide a more comprehensive understanding of the structure's condition, especially when discrepancies between design documentation and as-built conditions arise. These technologies not only reduce operational costs by eliminating the need for heavy machinery or scaffolding but also increase the safety of inspection teams and limit their exposure to hazardous on-site conditions.

Future research should aim to improve the accuracy and robustness of UAV photogrammetry, especially under adverse conditions such as high wind or in highly reflective environments. Moreover, the adoption of more advanced sensors, such as UAV-LiDAR, could further enhance the precision of remote measurements, particularly in areas with complex geometries or limited access. Additionally, refining methods for integrating STS and UAV data will be essential for the widespread adoption of these technologies in structural health monitoring (SHM) applications.

References

1. Cabral, R.; Oliveira, R.; Ribeiro, D.; Rakoczy, A.M.; Santos, R.; Azenha, M.; Correia, J. Railway Bridge Geometry Assessment Supported by Cutting-Edge Reality Capture Technologies and 3D As-Designed Models. *Infrastructures* **2023**, *8*, 114. [CrossRef]
2. Nepomuceno, D.T.; Bennetts, J.; Pregnolato, M.; Tryfonas, T.; Vardanega, P.J. Development of a Schema for the Remote Inspection of Bridges. *Proc. Inst. Civ. Eng.—Bridge Eng.* **2022**, 1–16. [CrossRef]
3. Galdelli, A.; D'Imperio, M.; Marchello, G.; Mancini, A.; Scaccia, M.; Sasso, M.; Frontoni, E.; Cannella, F. A Novel Remote Visual Inspection System for Bridge Predictive Maintenance. *Remote Sens.* **2022**, *14*, 2248. [CrossRef]
4. Ribeiro, D.; Santos, R.; Cabral, R.; Calçada, R. Remote Inspection and Monitoring of Civil Engineering Structures Based on Unmanned Aerial Vehicles. In *Advances on Testing and Experimentation in Civil Engineering*; Chastre, C., Neves, J., Ribeiro, D., Neves, M.G., Faria, P., Eds.; Springer Tracts in Civil Engineering; Springer International Publishing: Cham, Switzerland, 2023; pp. 123–144. ISBN 978-3-031-23887-1.
5. Nguyen, D.-C.; Nguyen, T.-Q.; Jin, R.; Jeon, C.-H.; Shim, C.-S. BIM-Based Mixed-Reality Application for Bridge Inspection and Maintenance. *Constr. Innov.* **2021**, *22*, 487–503. [CrossRef]

6. Gaspari, F.; Ioli, F.; Barbieri, F.; Belcore, E.; Pinto, L. Integration of UAV-Lidar and UAV-Photogrammetry for Infrastructure Monitoring and Bridge Assessment. *Int. Arch. Photogramm. Remote Sens. Spat. Inf. Sci.* **2022**, *43*, 995–1002. [CrossRef]

7. Owerko, P.; Owerko, T. Novel Approach to Inspections of As-Built Reinforcement in Incrementally Launched Bridges by Means of Computer Vision-Based Point Cloud Data. *IEEE Sens. J.* **2021**, *21*, 11822–11833. [CrossRef]

8. Rakoczy, A.M.; Ribeiro, D.; Hoskere, V.; Narazaki, Y.; Olaszek, P.; Karwowski, W.; Cabral PhD Student, R.; Guo, Y.; Futai, M.M.; Milillo, P.; et al. Technologies and Platforms for Remote and Autonomous Bridge Inspection—Review. *Structural Engineering International* **2024**, 1–23. [CrossRef]

9. Hines, J.; Rashidi, A.; Brilakis, I. Distance Measurement in the AEC/FM Industry: An Overview of Technologies. In Proceedings of the 5th International Conference on Construction Engineering and Project Management, Taipei, Taiwan, 28–30 August 2014.

10. Scherer, M.; Lerma, J.L. From the Conventional Total Station to the Prospective Image Assisted Photogrammetric Scanning Total Station: Comprehensive Review. *J. Surv. Eng.* **2009**, *135*, 173–178. [CrossRef]

11. Omidalizarandi, M.; Kargoll, B.; Paffenholz, J.-A.; Neumann, I. Accurate Vision-Based Displacement and Vibration Analysis of Bridge Structures by Means of an Image-Assisted Total Station. *Adv. Mech. Eng.* **2018**, *10*, 168781401878005. [CrossRef]

12. Ehrhart, M.; Kalenjuk, S.; Lienhart, W. Monitoring of Bridge Vibrations with Image-Assisted Total Stations. In Proceedings of the 4th Conference on Smart Monitoring, Assessment and Rehabilitation of civil Structures (SMAR), Zurich, Switzerland, 13–15 September 2017.

13. Sanchez-Cuevas, P.J.; Ramon-Soria, P.; Arrue, B.; Ollero, A.; Heredia, G. Robotic System for Inspection by Contact of Bridge Beams Using UAVs. *Sensors* **2019**, *19*, 305. [CrossRef]

14. Grimm, D.E. Leica Nova MS50: The World's First MultiStation. *GeoInformatics* **2013**, *16*, 22.

15. Olaszek, P.; Maciejewski, E.; Rakoczy, A.; Cabral, R.; Santos, R.; Ribeiro, D. Remote Inventory and Inspection of the Truss Bridge Elements and Connections Using STS and UAV. In Proceedings of the XLIV Ibero-Latin American Congress on Computational Methods in Engineering, Porto, Portugal, 13–16 November 2023; Volume 5.

16. Azeez, A.K. Deformation Monitoring Using Total Stations: An Evaluation of System Performance. *J. Geomat. Environ. Res* **2018**, *1*, 1–13.

17. Onu, C. Current Trends on Monitoring the Deformations of Studied Constructions. *RevCAD Univ.* **2011**, *1*, 169–178.

18. Liu, X.; Wei, S.Y.; Gao, Q.; Qing, Z.; Ran, C.L. Subway Monitoring System Based on TM30 Georobot Research and Implementation. *AMR* **2011**, *368–373*, 2109–2116. [CrossRef]

19. Zeidan, Z.; Beshr, A.; Sameh, S. Precision Comparison and Analysis of Reflector-Less Total Station Observations. *Bull. Fac. Engineering. Mansoura Univ.* **2020**, *40*, 86–97. [CrossRef]

20. Shakarji, C.M.; Srinivasan, V. Fitting Weighted Total Least-Squares Planes and Parallel Planes to Support Tolerancing Standards. In Proceedings of the 32nd Computers and Information in Engineering Conference, Parts A and B, Chicago, IL, USA, 12–15 August 2012; Volume 2, pp. 449–459.

21. Fawzy, H.E.-D. Evaluate the Accuracy of Reflector-Less Total Station. *Int. J. Civ. Eng. Technol.* **2015**, *6*, 23–30.

22. Haddad, N.; Ishakat, F. 3D Laser Scanner and Reflectorless Total Station: A Comparative Study of the Slots of El-Khazneh at Petra in Jordan. *Int. Arch. Photogramm. Remote Sens. Spat. Inf. Sci.* **2007**, *36*, C53.

23. Nwaogu, J.M.; Yang, Y.; Chan, A.P.C.; Chi, H. Application of Drones in the Architecture, Engineering, and Construction (AEC) Industry. *Autom. Constr.* **2023**, *150*, 104827. [CrossRef]

24. Montes, K.M.; Dang, J.; Liu, J.; Chun, P. Bridge Status Realization and Management Enhanced by UAV, SfM, and Deep Learning. In *Proceedings of the European Workshop on Structural Health Monitoring*; Rizzo, P., Milazzo, A., Eds.; Springer International Publishing: Cham, Switzerland, 2023; pp. 536–545.

25. Cabral, R.; Ribeiro, D.; Rakoczy, A. Engineering the Future: A Deep Dive into Remote Inspection and Reality Capture for Railway Infrastructure Digitalization. In *Digital Railway Infrastructure*; Ribeiro, D., Montenegro, P.A., Andersson, A., Martínez-Rodrigo, M.D., Eds.; Springer Nature: Cham, Switzerland, 2024; pp. 229–256. ISBN 978-3-031-49589-2.

26. Li, Z.; Shan, J. RANSAC-Based Multi Primitive Building Reconstruction from 3D Point Clouds. *ISPRS J. Photogramm. Remote Sens.* **2022**, *185*, 247–260. [CrossRef]

27. CloudCompare—Home. Available online: https://www.cloudcompare.org/main.html (accessed on 10 August 2023).

28. Software. Available online: https://leica-geosystems.com/en-us/products/laser-scanners/software (accessed on 24 October 2024).

29. iTwin Platform | Bentley Systems | Infrastructure Software. Available online: https://www.bentley.com/software/itwin-platform/ (accessed on 24 October 2024).

30. ReCap Pro 2025 Features | Autodesk. Available online: https://www.autodesk.com/products/recap/features (accessed on 24 October 2024).

31. MathWorks—Maker of MATLAB and Simulink. Available online: https://www.mathworks.com/ (accessed on 24 October 2024).

32. Autodesk Empowers Innovators Everywhere to Make the New Possible. Available online: https://www.autodesk.com/ (accessed on 24 October 2024).

33. Băncilă, R.; Feier, A.; Petzek, E. Proposals for the Application of the European Standard SR-EN-1090 in the Design and Execution of Steel Structures Especially Bridges. *AMR* **2016**, *1138*, 95–100. [CrossRef]